



# Investigation of Microscale Laser Shock Flat Hole Clinching

Yaxuan Hou<sup>1</sup> · Kexin Ding<sup>1</sup> · Guoxin Lu<sup>1</sup> · Chao Zheng<sup>1</sup> · Zhong Ji<sup>1</sup>

Received: 10 January 2022 / Revised: 24 March 2022 / Accepted: 20 April 2022 / Published online: 26 July 2022  
© The Author(s), under exclusive licence to Korean Society for Precision Engineering 2022

## Abstract

This paper proposes an improved laser shock flat hole clinching process for joining ductile and brittle materials to obtain single-sided flat joints in microscale. A copper foil is clinched with a perforated sheet and a mechanical joining is achieved by this process. Experiments and numerical simulations are conducted for three thickness combinations of 50  $\mu\text{m}$ /50  $\mu\text{m}$ , 30  $\mu\text{m}$ /50  $\mu\text{m}$  and 20  $\mu\text{m}$ /100  $\mu\text{m}$  to investigate the joinability of this process. The results show that a step-by-step laser shock process with a low-energy pre-shock and a high-energy secondary shock can effectively join the copper foil and the perforated sheet. The three thickness combinations of the upper and lower sheets result in three clinching structures, namely stacked, intermediate and thinning joints. And the joint strength mainly depends on the thinner sheet in a successful joining even for the single joint or the double-joint.

**Keywords** Laser shock flat hole clinching · Joining · Clinching structure · Joint strength

## 1 Introduction

In order to expand the applications of the clinching technology, the external protrusions on the clinched joints should be avoided as much as possible. Borsellino [1] introduced a new joining technique called flat clinching to make mechanical joints without anvil-sided protrusions and compared the joint strength among various joining processes. Neugebauer [2] found that the die-less clinching technology can produce a single-sided flat joining, which could be used in visible or functional areas. Gerstmann [3] adopted the finite element method (FEM) to simulate a flat clinching process and quantified the related technical parameters. Han [4] used an orthogonal experimental method to optimize the tool parameters of flat clinching. Chen [5] used a reshaping rivet to reduce the protrusion height and to increase the strength of clinched joints, they also examined the effects of sheet arrangements on the flat clinching processes. Wen [6, 7] developed a flat hole-clinching technique to achieve a flat joining between two layers of materials, in which a punch was used to force the upper sheet flowing into the hole of

the lower sheet, and an interlock between the hole and the sheet was deformed, and the two sheets were finally joined together. Although the flat clinching so far can be used to join similar or dissimilar sheet materials, it is a bit difficult to join ultrathin sheets in microscale due to the limitations of tooling accuracy.

Laser shock forming (LSF) was developed on the basis of laser shock hardening. It utilized shock waves induced by pulsed laser as a driving force to promote plastic deformation. Laser shock clinching (LSC) combined LSF and mechanical joining technology, which can break through the limitations of conventional clinching in the field of microscale joining. The basic concepts and principles of LSC were first proposed by Ji [8]. Veenaas [9, 10] used the TEA-CO<sub>2</sub> laser to realize a microscopic joining of aluminum foil and stainless steel. Wang [11, 12] explored the LSC of similar or dissimilar materials and successfully clinched non-ferrous metal foils with perforated sheets. You [13] presented a technique called incremental laser shock forming, in which the pulsed laser was used to plastically deform a linear undercut structure. Zheng [14, 15] investigated the joining behavior and the effect of process parameters for laser shock hole-clinching of a single thickness of Cu–Fe. However, in previous studies, different material thickness combinations corresponding to different forming mechanisms received less attention. Moreover, the resulting mechanical joints

✉ Zhong Ji  
jizhong@sdu.edu.cn

<sup>1</sup> School of Materials Science and Engineering, Shandong University, 17923 Jingshi Road, Jinan 250061, Shandong, People's Republic of China

had geometric protrusions, which were limited in terms of microscale visibility and usability.

This paper proposes a microscale improved laser shock flat hole clinching (LSFHC) process for joining two metal sheets, especially for ductile and brittle materials. A copper foil and a perforated stainless steel sheet were joined by this process to obtain single-sided flat joints, which eliminates the geometric protrusions. The joinability of this process for three thickness combinations was investigated by experiments and numerical simulations, and the joint strength was verified by single-lap shear tests.

## 2 Experimental Setup

The LSFHC process is a clinching method for joining two layers of metal sheets, especially for joining ductile and brittle materials, as shown in Fig. 1. In this process, the Nd:YAG laser system was used to produce the laser beams, and its specific parameters were shown in Table 1. When the high-energy laser beams passed through the confinement layer (usually a quartz glass) and reached the upper surface of the ablative layer (usually a black paint), the ablative layer instantly absorbed the laser energy and ionized and decomposed, transforming into the laser induced shock waves. A lower sheet with a prefabricated conical through-hole is made of a brittle material (e.g., stainless steel sheet) on the top of which an upper sheet made of a ductile material (e.g., copper foil) is placed. Under the action of laser induced shock waves, the upper sheet flows into the cavity of the prefabricated hole in the lower sheet to form a geometric interlock.

The 20 mm square T2 pure copper foils were used as the upper sheet, which was cleaned in an ultrasonic alcohol bath and then annealed in a vacuum furnace to eliminate the effect of the rolling direction. 20 mm square 304 stainless steel sheets with prefabricated conical through-holes were used as the brittle material for the lower sheet. The specific parameters of the perforated sheets were listed in Table 2.

The thicknesses of the upper and lower sheets are  $t_U$  and  $t_L$ , respectively. Three  $t_U/t_L$  combinations, namely

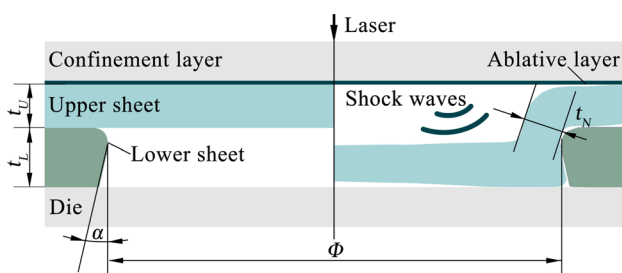


Fig. 1 The LSFHC process

Table 1 Specific parameters of the laser system

Requirement	Parameter
Output wavelength	1064 ± 1 nm
Output energy	0.8–6 J
Repetition frequency	1 Hz
Pulse width	~ 12 ns
Spot diameter	~ 6 mm
Light spot space profile	Almost flat top distribution

50 μm/50 μm, 30 μm/50 μm and 20 μm/100 μm were designed in this study. After the LSFHC process, the cross-sectional views of joints were observed under a 4XC-PC microscope to confirm the joining results.

## 3 Simulation Preparation

A three-dimensional numerical model was established in the finite element simulation software ABAQUS. In this paper, the Johnson–Cook constitutive model, which is commonly used to describe the deformation process of high strain rate metallic materials, is used to simulate the flow and deformation behavior of the copper foil. The yield stress of von-Mises can be expressed as [16]:

$$\sigma_y = (A + B\bar{\epsilon}^n)(1 + C \ln \bar{\epsilon}^*) (1 - (T^*)^m) \quad (1)$$

where  $\sigma_y$  is the equivalent stress,  $\bar{\epsilon}$  is the equivalent plastic strain,  $A$ ,  $B$ ,  $C$ ,  $m$ , and  $n$  are all material constants,  $\bar{\epsilon}^*$  is the strain rate,  $T^* = (T - T_0)/(T_m - T_0)$ ,  $T_0$  is the room temperature,  $T_m$  is the melting point of the material. Specific parameters can be referred to the literature [11].

The Fabbro model is usually used to simulate the propagation of the laser shock waves in a constrained mode [17]. The model assumes that the laser energy is uniformly distributed and the material surface is uniformly heated within the range of the light spot. Both the constrained layer and the target are isotropic homogeneous materials with a constant thermophysical property. The plasma is an ideal gas that expands only in the axial direction. The peak shock wave pressure can be evaluated by the formula:

Table 2 The specific parameters of the perforated sheets

Parameter	Value
The upper diameter of the conical hole ( $\Phi$ /mm)	0.8
The taper angle ( $\alpha$ /°)	10
The diameter-depth ratio ( $r$ )	8,16

$$P = 0.01\sqrt{\beta/(2\beta + 3)} \cdot Z \cdot I_0 \tag{2}$$

where  $P$  is the peak pressure of the shock wave,  $\beta$  is the transformation coefficient, here  $\beta = 0.1$ .  $Z$  is the combined acoustic impedance of the target and the constraint layer, where  $Z = 2 \times 10^6 \text{ g cm}^{-2} \text{ s}^{-1}$ ,  $I_0$  is the laser power density, expressed as:  $I_0 = 4E/\pi d^2 \tau$ .  $E$  is the laser energy,  $d$  is the laser spot diameter,  $\tau$  is the laser pulse width, here  $\tau = 12 \text{ ns}$ . The specific peak pressures are listed in Table 3.

The shock wave has a short action time, so the curve of the laser shock wave pressure with time can be simplified to a triangular pulse. Generally speaking, the duration of the shock wave in the constrained model is about 2–3 times the laser pulse width. In this paper, the duration of the shock wave is 36 ns, and the peak pressure is reached at 12 ns. In addition, the shock wave pressure presents a Gaussian distribution in space with the following:  $P(a, t) = P(t)e^{-2a^2/d^2}$ , where  $a$  is the radial distance from any position to the center of the spot.

### 4 Joinability of LSFHC Process

After the preview experiments, it was found that due to the limitation of the laser energy, a single shock did not form a better clinching structure, so a step-by-step forming method with a low-energy pre-shock and a high-energy secondary shock was developed. Figure 2 illustrated the process windows with cross-sectional views of the successfully clinched specimens, where the laser energies for the pre-shock and

the secondary shock were expressed by the horizontal and vertical axes, respectively. The minimum laser energy required for successful clinching was marked in red.

As can be observed in Fig. 2, each combination of 50  $\mu\text{m}/50 \mu\text{m}$  and 30  $\mu\text{m}/50 \mu\text{m}$  presented two joining results: successful clinching and incomplete forming. In the energy range used in this experiment, no material failure occurred. The combination of 20  $\mu\text{m}/100 \mu\text{m}$  presented four joining results: successful clinching, incomplete forming, the copper foil damaged after pre-shock, and damaged after secondary shock. Figure 3 displayed some of the above specimens.

A numerical model was developed and compared with the experimental clinching structures, which was presented in Fig. 4. In general, the experimental and simulation results are in good consistency with a dimensional error of 2.32%. However, it is still noted that there are some differences between them. This may be due to the deviation of the material parameters and the inaccuracy of the relevant calculation equations. Figure 5 illustrated the specific deformation process. Combining the experimental and simulated results, it was found that the deformation of the copper foil all went

**Table 3** Specific peak pressures used in the simulation

Thickness combination	Value
50 $\mu\text{m}/50 \mu\text{m}$	2.85 GPa + 3.32 GPa
30 $\mu\text{m}/50 \mu\text{m}$	2.63 GPa + 3.21 GPa
20 $\mu\text{m}/100 \mu\text{m}$	1.72 GPa + 2.35 GPa

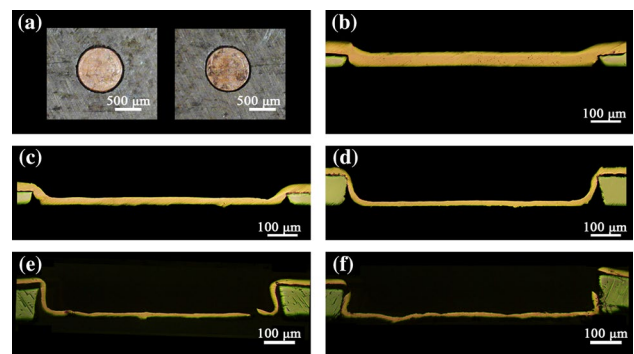


**Fig. 3** Specimens in the LSFHC process. **a** Surface profiles of joints; **b–d** incomplete forming in 50  $\mu\text{m}/50 \mu\text{m}$ , 30  $\mu\text{m}/50 \mu\text{m}$  and 20  $\mu\text{m}/100 \mu\text{m}$ ; **e–f** material failures in 20  $\mu\text{m}/100 \mu\text{m}$

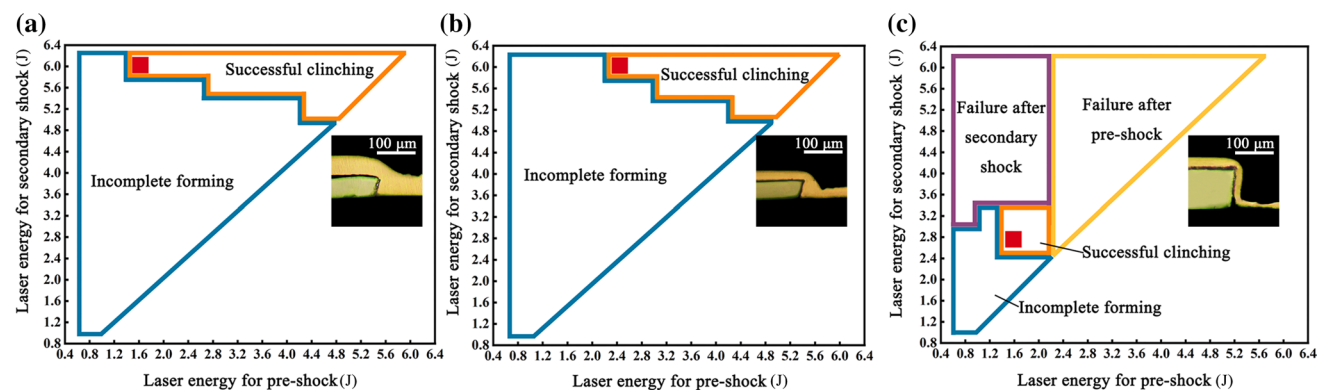


**Fig. 2** The clinching process windows. **a** 50  $\mu\text{m}/50 \mu\text{m}$ ; **b** 30  $\mu\text{m}/50 \mu\text{m}$ ; **c** 20  $\mu\text{m}/100 \mu\text{m}$

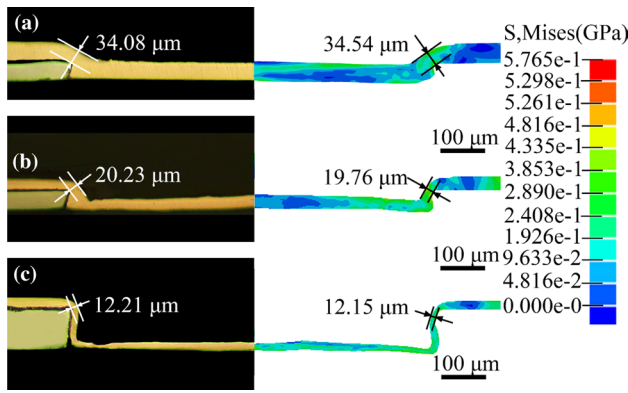


**Fig. 4** Comparison of clinching structures in experimental and simulation results. **a** 50  $\mu\text{m}/50 \mu\text{m}$ ; **b** 30  $\mu\text{m}/50 \mu\text{m}$ ; **c** 20  $\mu\text{m}/100 \mu\text{m}$

through the following three stages: free bulging, reverse plastic deformation after the center of the platform hit the bottom support, and radial deformation until the joint was formed.

However, by observing the cross-sectional views of the joints and comparing the deformation process, different forming mechanisms were detected, which correspond to three clinching structures. For 50  $\mu\text{m}/50 \mu\text{m}$ , the clinching structure showed a stacked joint as shown in Figs. 4a and 5a. The copper foil was thick enough that it was extruded into the conical hole to form an interlock. For 20  $\mu\text{m}/100 \mu\text{m}$ , the clinching structure appeared as a thinning joint as displayed in Figs. 4c and 5c. The copper foil engaged in the forming was relatively thin and flowed severely, so the joint was formed by thinning and bulging. Meanwhile, it was observed that the geometric interlock was very poor. For 30  $\mu\text{m}/50 \mu\text{m}$ , the clinching structure appeared as an intermediate joint as shown in Figs. 4b and 5b. The above two situations coexisted in the intermediate joint, but stacking was dominant.

### 5 Strength of LSFHC Joints

To evaluate the strength of joints, single-lap shear tests were performed on the formed parts. Five load–displacement curves with similar shapes and values were selected as the final results. Figure 6a exhibited the specific dimensions of the single-joint specimen. Figure 7 showed the single-joint curves for different combinations. In microscale forming, the strength of a single joint is lower because of the smaller joint size and smaller load-bearing area. In practice, multiple joints are mostly employed to ensure joint strength. Therefore, in addition to the single joint, the vertical and horizontal double-joint specimens were also considered, as presented in Fig. 6b, c, and the corresponding load–displacement curves were displayed in Figs. 8 and 9.

The load–displacement curves had two main shapes: one was an approximately linear shape. In the case of a single joint and the 20  $\mu\text{m}/100 \mu\text{m}$ , the curve increased rapidly to

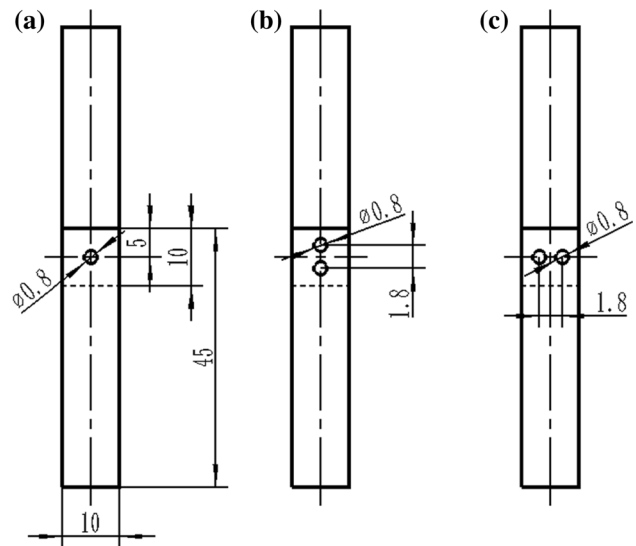


**Fig. 6** Specific dimensions of the specimens in single-lap shear tests. **a** The single joint; **b** the vertical double-joint; **c** the horizontal double-joint

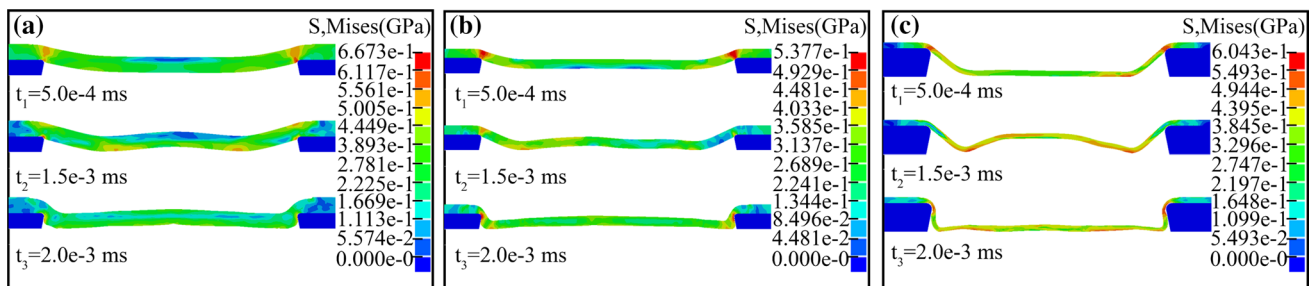


**Fig. 5** Simulation of the LSFHC process. **a** 50  $\mu\text{m}/50 \mu\text{m}$ ; **b** 30  $\mu\text{m}/50 \mu\text{m}$ ; **c** 20  $\mu\text{m}/100 \mu\text{m}$



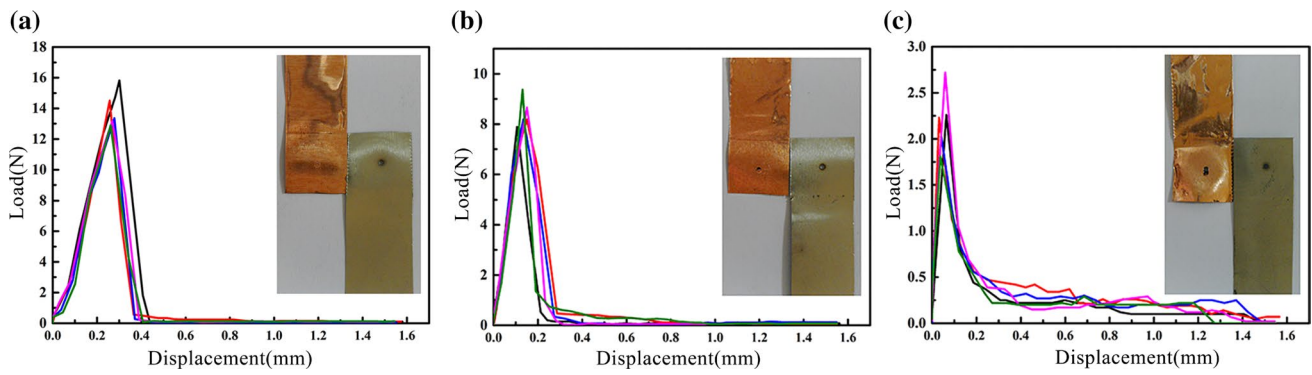


**Fig. 7** Load–displacement curves of the single joint. **a** 50  $\mu\text{m}/50 \mu\text{m}$ ; **b** 30  $\mu\text{m}/50 \mu\text{m}$ ; **c** 20  $\mu\text{m}/100 \mu\text{m}$

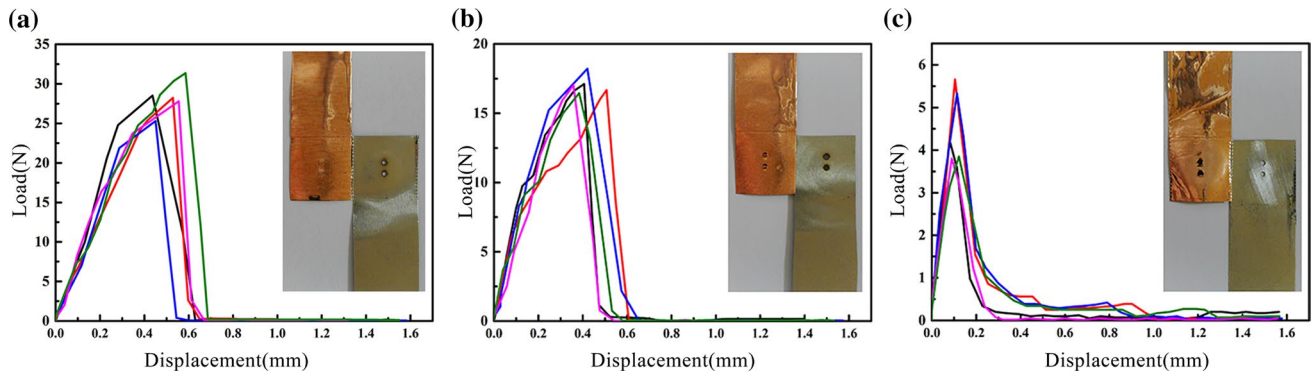


**Fig. 8** Load–displacement curves of the vertical double-joint. **a** 50  $\mu\text{m}/50 \mu\text{m}$ ; **b** 30  $\mu\text{m}/50 \mu\text{m}$ ; **c** 20  $\mu\text{m}/100 \mu\text{m}$

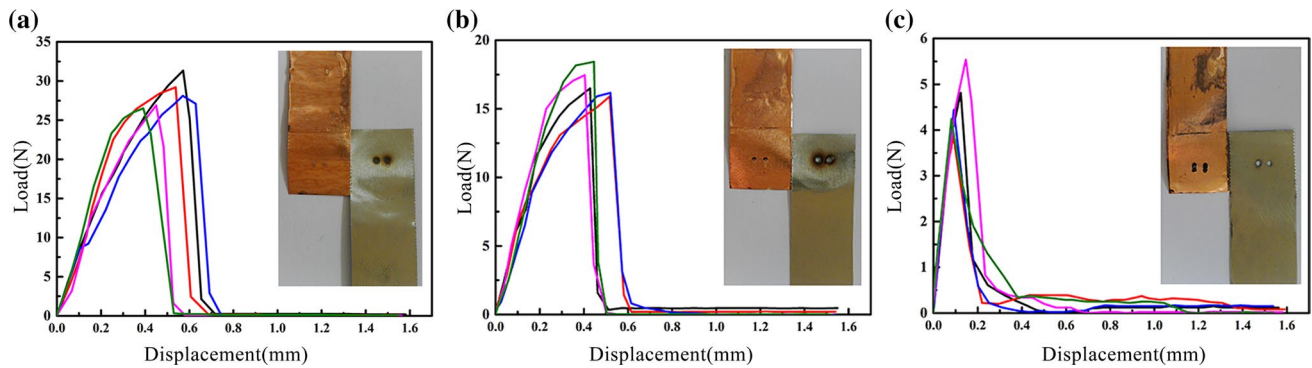


**Fig. 9** Load–displacement curves of the horizontal double-joint. **a** 50  $\mu\text{m}/50 \mu\text{m}$ ; **b** 30  $\mu\text{m}/50 \mu\text{m}$ ; **c** 20  $\mu\text{m}/100 \mu\text{m}$

the peak and then decreased quickly. This was because the copper foil was in the linear elastic deformation stage under the tensile load. When the load reached the strength limit of the joint, the joint failed and the curve decayed immediately. The other was that the curve first rose in an approximately linear shape, and then the slope of the curve decreased until it reached the peak load, and the curve decayed rapidly. It was mainly seen in the double-joint of the 50  $\mu\text{m}/50 \mu\text{m}$  and

the 30  $\mu\text{m}/50 \mu\text{m}$ . The slope of the curve changes from large to small, which means that plastic deformation occurs during the deformation process.

Figure 10 showed the average values of the peak loads in the above curves, reflecting the joint strength for different combinations and joint alignments. It could be seen more intuitively that the strength of the double-joint is greater, about twice that of the single joint. And there was little

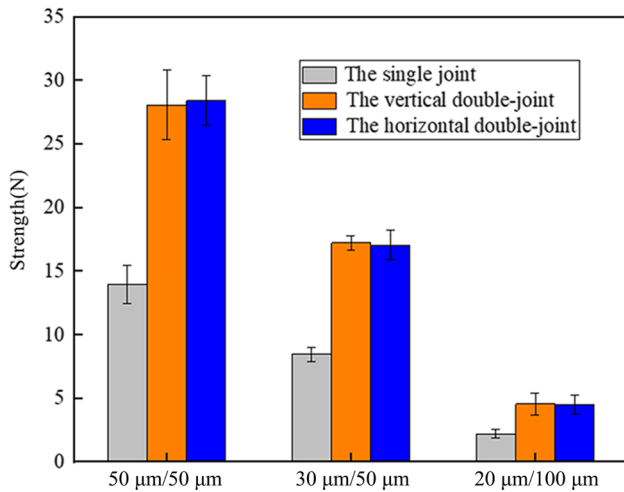


**Fig. 10** Average peak loads for different combinations

difference between the joint strength of the vertical double-joint and the horizontal double-joint. It indicates that the joint strength is mainly determined by the bearing area of the joints, and the larger the bearing area, the greater the joint strength. Moreover, the alignment of the double joints, either vertically or horizontally, has no significant effect on the joint strength. Besides, the highest joint strength was found in 50 μm/50 μm, followed by 30 μm/50 μm and the lowest in 20 μm/100 μm for both single and double joints. It shows that in the LSFHC process, the strength of the successfully interlocked joint depends on the thinner one of the upper and lower sheets.

## 6 Conclusion and Outlook

In this paper, the LSFHC process is proposed to realize the joining of ductile and brittle materials, which provides a feasible solution for the existing microscale joining in visible or functional areas. Taking the copper foil and stainless steel sheets as examples, the joining results, forming mechanisms, clinching structures and joint strength were investigated for three combinations. The main conclusions are as follows:

1. The LSFHC process can join a copper foil to a perforated sheet and create a single-sided flat joint in microscale. Effective clinching can be obtained for thickness combinations of 50 μm/50 μm, 30 μm/50 μm, and 20 μm/100 μm.
2. The three thickness combinations of the upper and lower sheets result in three forming mechanisms corresponding to three types of clinching structures: stacked, intermediate and thinning joints.

3. The joint strength is mainly determined by the bearing area of the joints, the larger the bearing area, the greater the joint strength. The alignment of double joints, either vertically or horizontally, has no significant influence on the joint strength. The strength of a successful interlocking joint depends on the thinner one of the upper and lower sheets.
4. Based on the research in this paper, the specific effects of geometry parameters on the clinching structures and the joint strength can be further explored in the case of double joints, such as the diameter-depth ratio and the distance between holes of the perforated sheet, and other factors.

**Acknowledgements** This work is supported by the National Natural Science Foundation of China (Nos. 52075298, 51801031, 51575314, 52075299) and the Fund of the State Key Laboratory of Solidification Processing in NPU (No. SKLSP202014).

## Declarations

**Conflict of interest** The authors have no relevant financial or non-financial interests to disclose.

## References

1. Borsellino, C., Di Bella, G., & Ruisi, V. F. (2007). Study of new joining technique: Flat clinching. *Key Engineering Materials*, 344, 685–692. <https://doi.org/10.4028/www.scientific.net/KEM.344.685>
2. Neugebauer, R., Todtermuschke, M., Mauermann, R., & Riedel, F. (2008). Overview on the state of development and the application potential of dieless mechanical joining processes. *Archives of Civil and Mechanical Engineering*, 8, 51–60. [https://doi.org/10.1016/S1644-9665\(12\)60121-6](https://doi.org/10.1016/S1644-9665(12)60121-6)
3. Gerstmann, T., & Awiszus, B. (2014). Recent developments in flat-clinching. *Computational Materials Science*, 81, 39–44. <https://doi.org/10.1016/j.commatsci.2013.07.013>
4. Han, X., Zhao, S., Chen, C., Liu, C., & Xu, F. (2017). Optimization of geometrical design of clinching tools in flat-clinching. *Proceedings of the Institution of Mechanical Engineers, Part C: Journal of Mechanical Engineering Science*, 231, 4012–4021. <https://doi.org/10.1177/0954406216660335>
5. Chen, C., Zhao, S., Han, X., Cui, M., & Fan, S. (2016). Optimization of a reshaping rivet to reduce the protrusion height and increase the strength of clinched joints. *Journal of Materials Processing Technology*, 234, 1–9. <https://doi.org/10.1016/j.jmatp.2016.03.006>
6. Wen, T., Wang, H., Yang, C., & Liu, L. (2014). On a reshaping method of clinched joints to reduce the protrusion height. *The International Journal of Advanced Manufacturing Technology*, 71, 1709–1715. <https://doi.org/10.1007/s00170-014-5612-2>
7. Wen, T., Huang, Q., Liu, Q., Ou, W., & Zhang, S. (2016). Joining different metallic sheets without protrusion by flat hole clinching process. *The International Journal of Advanced Manufacturing Technology*, 85, 217–225. <https://doi.org/10.1007/s00170-015-7936-y>

8. Ji, Z., Liu, R., Wang, D., Zhang, M., & Su, Q. (2008). A micro clinching method and its device for joining ultra-thin sheets with pulsed laser. *Chinese Patent*. ZL200810014018.1.
9. Veenaas, S., & Vollertsen, F. (2014). High speed joining by laser shock forming. *Advanced Materials Research*, 966–967, 597–606. <https://doi.org/10.4028/www.scientific.net/AMR.966-967.597>
10. Veenaas, S., Wielage, H., & Vollertsen, F. (2014). Joining by laser shock forming: Realization and acting pressures. *Production Engineering*, 8, 283–290. <https://doi.org/10.1007/s11740-013-0521-z>
11. Wang, X., Ji, Z., Wang, J., You, S., Zheng, C., & Liu, R. (2018). An experimental and numerical study on laser shock clinching for joining copper foil and perforated stainless steel sheet. *Journal of Materials Processing Technology*, 258, 155–164. <https://doi.org/10.1016/j.jmatprotec.2018.03.025>
12. Wang, X., Ji, Z., Zheng, C., & Liu, R. (2020). Joining similar and dissimilar material combinations by laser shock forming. *Journal of Manufacturing Processes*, 60, 318–327. <https://doi.org/10.1016/j.jmapro.2020.10.067>
13. You, S., Wang, X., Ji, Z., Zheng, C., Zhang, G., & Liu, R. (2019). Making line undercut structure by incremental laser shock forming. *International Journal of Precision Engineering and Manufacturing*, 20, 1289–1296. <https://doi.org/10.1007/s12541-019-00141-w>
14. Zheng, C., Pan, C., Wang, J., Zhao, G., & Ji, Z. (2020). Mechanical joining behavior of Cu–Fe dissimilar metallic foils in laser shock clinching. *The International Journal of Advanced Manufacturing Technology*, 110, 1001–1014. <https://doi.org/10.1007/s00170-020-05920-8>
15. Zheng, C., Zhang, Y., Zhao, G., Ji, Z., & Sun, Y. (2020). Influence of process parameters on forming quality of Cu–Fe joints by laser shock hole-clinching. *The International Journal of Advanced Manufacturing Technology*, 110(3–4), 887–898. <https://doi.org/10.1007/s00170-020-05915-5>
16. Johnson, G. R., & Cook, W. H. (1983). A constitutive model and data for metals subjected to large strains, high strain rates and high temperatures. In *The 7th international symposium on ballistics*.
17. Fabbro, R., Fournier, J., Ballard, P., Devaux, D., & Virmont, J. (1990). Physical study of laser-produced plasma in confined geometry. *Journal of Applied Physics*, 68, 775–784. <https://doi.org/10.1063/1.346783>

**Publisher's Note** Springer Nature remains neutral with regard to jurisdictional claims in published maps and institutional affiliations.



**Yaxuan Hou** is a Ph.D. student in the School of Materials Science and Engineering at Shandong University. Her research interest is laser shock flat hole clinching.



**Kexin Ding** is a master student in the School of Materials Science and Engineering at Shandong University. Her research is laser shock clinching.



**Guoxin Lu** is an associate researcher in the School of Materials Science and Engineering at Shandong University. His research is on surface strengthening processing mechanism of aerospace materials.



**Chao Zheng** is a senior engineer in the School of Materials Science and Engineering at Shandong University. His research interests are advanced plastic forming theory and technology.



**Zhong Ji** is a professor in the School of Materials Science and Engineering at Shandong University. His research interests include laser processing and sheet metal forming.